Supplementary figures and table

Watanabe, M., J.-S. Kug, F.-F. Jin, M. Collins, M. Ohba, and A. T. Wittenberg (2012), Uncertainty in the ENSO amplitude change from the past to the future.

Table S1 List of the CMIP5 models and experiments used in this study.

		Ensemble size		Integration years
Model no.	Model name (alphabetical)	Historical run	RCP4.5 run	Pre-industrial run
1	BCC-CSM1	3	1	N/A
2	CanESM2	5	5	996
3	CNRM-CM5	10	1	850
4	CSIRO Mk-3.6	10	10	500
5	GFDL-CM3	5	1	500
6	GFDL-ESM2G	1	1	500
7	GFDL-ESM2M	1	1	500
8	GISS-E2-H	5	N/A	N/A
9	GISS-E2-R	5	5	N/A
10	HadCM3	9	N/A	N/A
11	HadGEM2-CC	1	1	240
12	INM-CM4	1	1	450
13	IPSL-CM5A-LR	3	3	800
14	IPSL-CM5A-MR	1	1	300
15	MIROC5	3	3	500
16	MPI-ESM-LR	3	3	1000
17	MRI-CGCM3	5	1	200
18	NorESM1-M	3	1	500

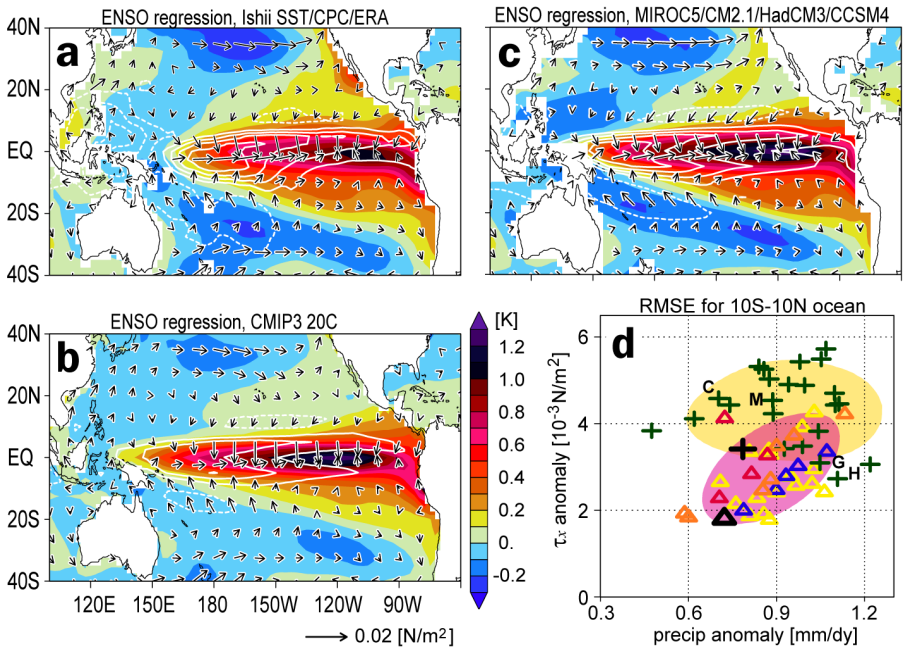

Figure S1 Patterns of El Niño and associated errors. (a) Anomalies of observed SST for 1945–2009 [*Ishii et al. 2006*] (colour), precipitation for 1979–2006 [*Xie and Arkin 1997*] (contour) and surface wind stresses for 1957–2002 [*Uppala et al. 2005*] (vector), regressed upon the monthly Niño 3 SST anomaly. (b) Ensemble average of the regressed anomalies for 24 CMIP3 GCMs. (c) Ensemble average of the combined parameter ensembles of four GCMs used in the present study. (d) RMS errors in the precipitation and zonal wind stress anomalies associated with ENSO (shown in b–c, but for individual models) over the equatorial Pacific (100° E–80° W, 10° S–10° N): CMIP3 models (green plus), MIROC5 (red), GFDL CM2.1 (blue), HadCM3 (yellow) and CCSM4 (orange). The thick plus and triangle indicate errors using the respective ensemble averages. The yellow and red shadings represent the 95% confidence limit of the χ^2 distribution estimated using a bootstrap method, fitted to CMIP3 MME and a combined PPE, respectively. The alphabets indicate the values from GFDL CM2.1 ('G'), HadCM3 ('H'), and old versions of MIROC ('M') and CCSM ('C') in CMIP3.

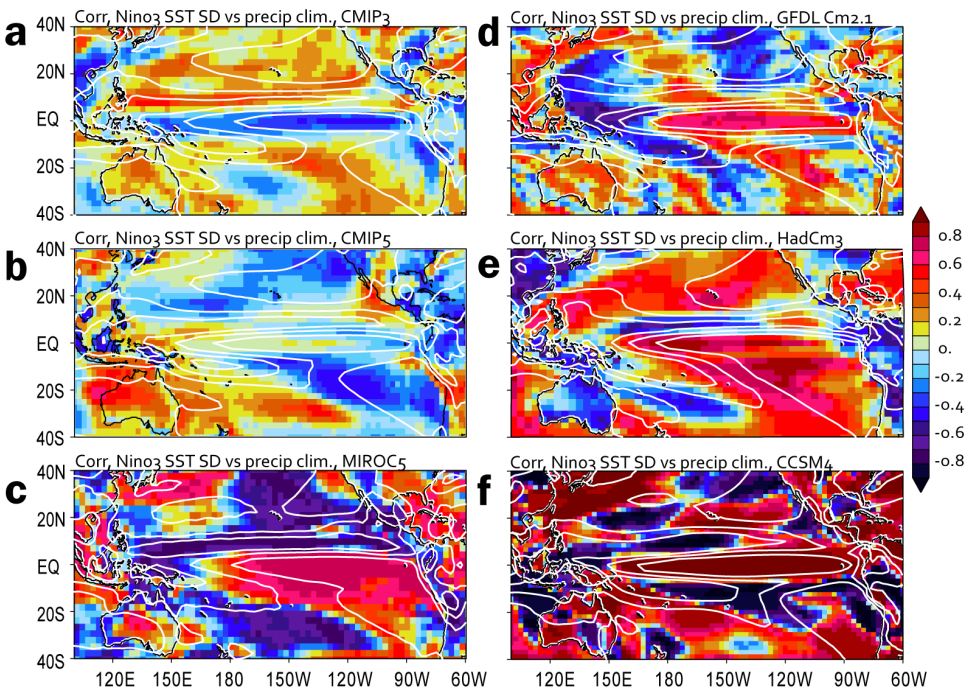

Figure S2 Correlation between ENSO amplitude and mean precipitation in model ensembles. (a) 24 CMIP3 models, (b) 18 CMIP5 models, (c) MIROC5 (4-member parameter ensemble), (d) GFDL CM2.1 (5-member parameter ensemble), (e) HadCM3 (17-member parameter ensemble) and (f) NCAR CCSM4 (7-member parameter ensemble). The ENSO amplitude is defined by the std dev of the Niño 3 SST anomaly, as in Fig. 1a. The white contours (2.5, 5, 7.5 mm dy^{-1}) indicate the ensemble average of the mean precipitation.

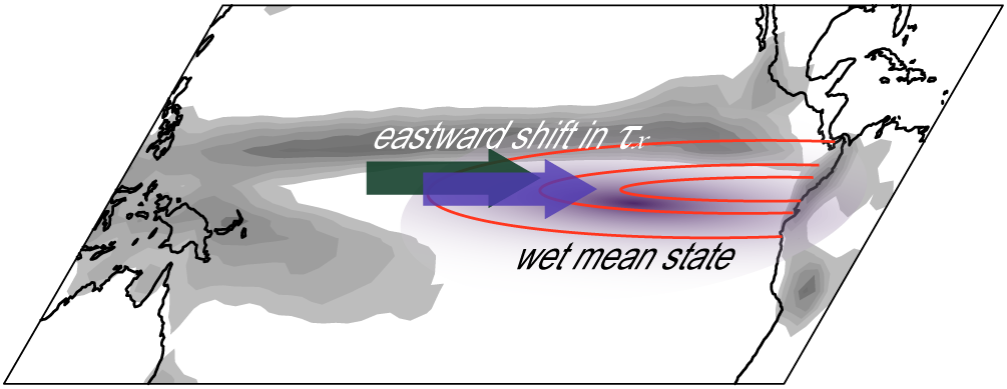

Figure S3 Schematic diagram showing the mean state controlling the ENSO amplitude. The grey shading indicates the mean precipitation pattern; red contours are typical SST anomalies during El Niño, and thick arrows represent the τ_x response to El Niño. A wetter mean condition over the central-eastern equatorial Pacific (blue shading) can make the precipitation response to occur, leading to the eastward shift in the τ_x response (green and blue arrows) [cf. *Watanabe et al. 2011, Kim et al. 2011*]. This strengthens the positive thermocline and zonal advective feedbacks, the latter due to in-phase occurrence between τ_x and SST anomalies, and hence acts to amplify ENSO [*Kang and Kug 2002*].

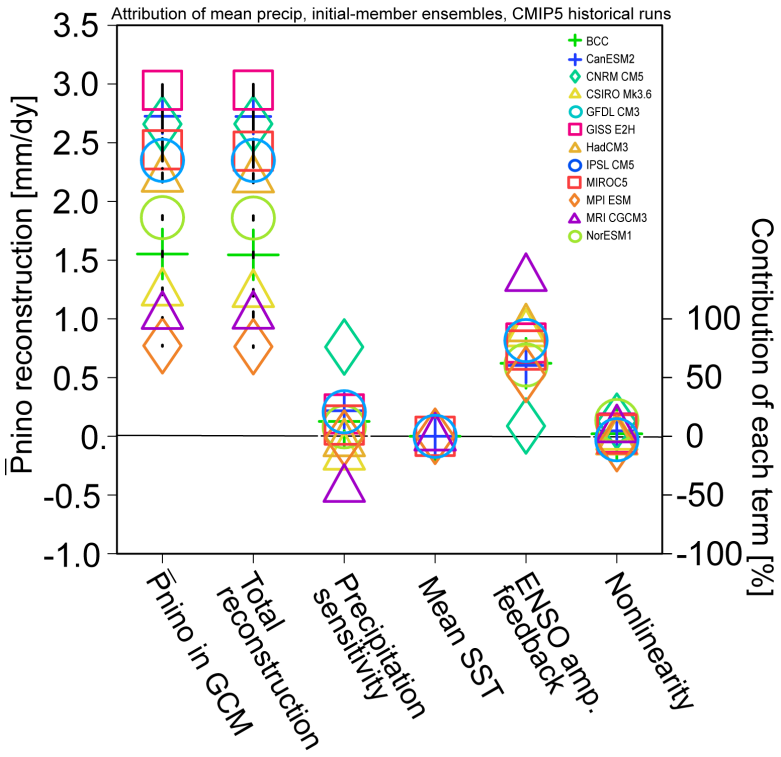

Figure S4 Same as Fig. 2 but for initial-member ensembles of the historical runs using 11 CMIP5 models. The notation of symbols follows Fig. 3b. Since the mean position changes in the SST PDF are too small to accurately estimate with these limited data lengths, the mean SST effect is set to zero by definition. The ENSO amplitude feedback accounts for 10-136 % in the 11 models, and the average of its contribution to $\overline{P}_{\text{niño}}$ is 72 %.

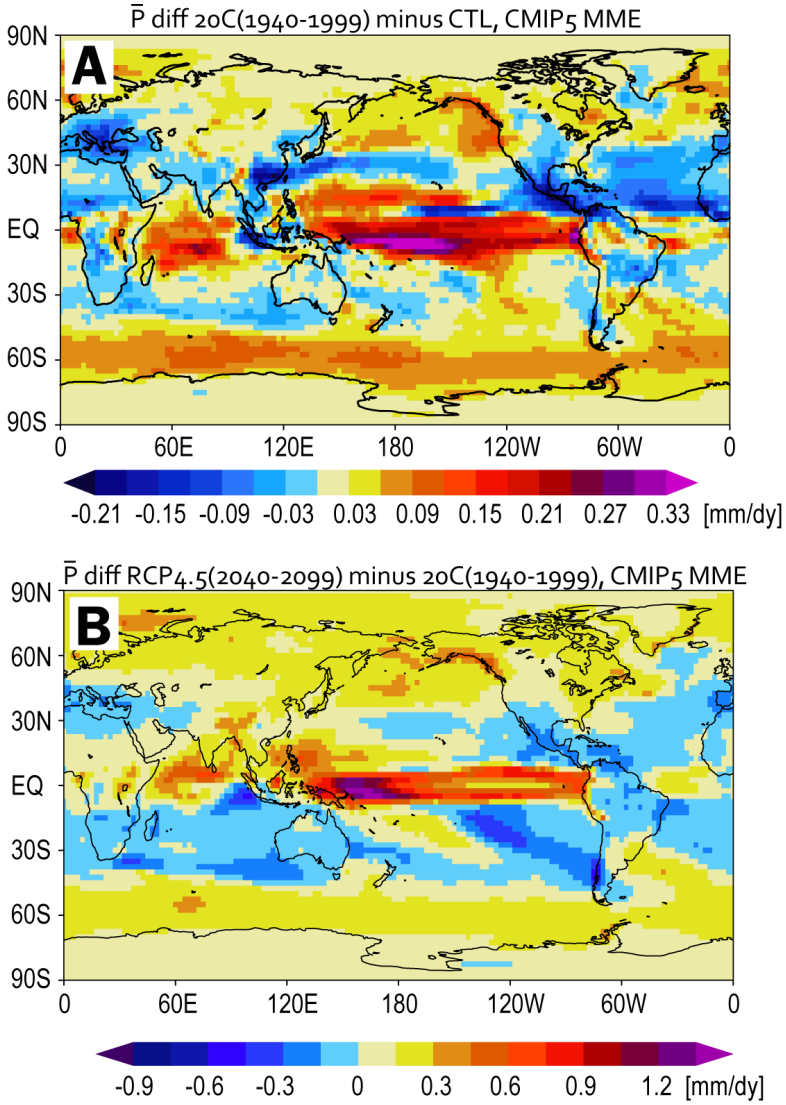

Figure S5 Changes in the ensemble-mean precipitation in CMIP5 MME from the past to present and to future, obtained from the $\bar{P}$ differences between (a) pre-industrial and historical (1940-1999) runs, and (b) historical (1940-1999) and the future scenario (2040-2099) runs. The future precipitation fields are derived from the RCP4.5 experiments [*Hibbard et al. 2011*].

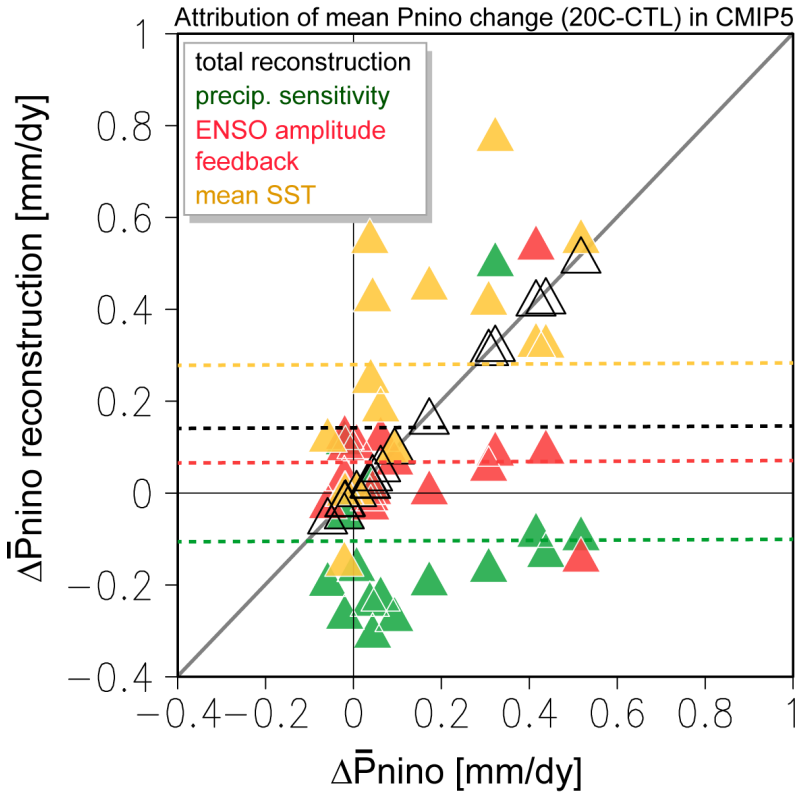

Figure S6 Scatterplot of the reconstructed $\Delta\overline{P}_{\text{niño}}$ following Eq. (1)-(2) against $\Delta\overline{P}_{\text{niño}}$ in the CMIP5 MME, corresponding values shown in Fig. 4a. The full reconstruction (black) and partial contributions by the changes in the precipitation sensitivity (green) and mean SST (orange), and the ENSO amplitude feedback (red) are shown for individual models. The multi-model means are indicated by dashed lines.

Additional references

Hibbard, K. A., D. P. van Vuuren, and J. Edmonds (2011), A primer on the Representative Concentration Pathways (RCPs) and the coordination between the climate and integrated assessment modeling communities. *CLIVAR Exchanges* **56**, 12-14.

Ishii, M., M. Kimoto, K. Sakamoto, and S. Iwasaki (2006), Steric sea level changes estimated from historical ocean subsurface temperature and salinity analyses. *J. Oceanogr.*, **62**, 155-170.

Kang, I.-S., and J.-S. Kug (2002), El Niño and La Niña sea surface temperature anomalies: Asymmetry characteristics associated with their wind stress anomalies. *J. Geophys. Res.*, **107**, doi:10.1029/2001JD000393

Kim, D., and Coauthors (2011), ENSO sensitivity to cumulus entrainment in a coupled GCM. *J. Geophys. Res.*, **116**, doi:10.1029/2011JD016526.

Uppala, S. M., and Coauthors (2005), The ERA-40 re-analysis. *Quart. J. Roy. Meteor. Soc.* **131**, 2961-3012.

Watanabe, M., M. Chikira, Y. Imada, and M. Kimoto (2011), Convective control of ENSO simulated in MIROC5. *J. Climate*, **24**, 543-562.

Xie, P., and P. A. Arkin (1997), Global precipitation: A 17-year monthly analysis based on gauge observations, satellite estimates, and numerical model outputs. *Bull. Amer. Meteor. Soc.*, **78**, 2539-2558.